Assessing composition and structure of soft biphasic media from Kelvin–Voigt fractional derivative model parameters

IOP Publishing Measurement Science and Technology
Meas. Sci. Technol. **28** (2017) 035703 (12pp) doi:10.1088/1361-6501/aa5531

Assessing composition and structure of soft biphasic media from Kelvin–Voigt fractional derivative model parameters[4]

Hongmei Zhang[1,2], Yue Wang[2], Mostafa Fatemi[3] and Michael F Insana[2]

[1] Key Laboratory of Biomedical Information Engineering, Ministry of Education, School of Life Science and Technology, Xi'an JiaoTong University, Xianning West Road No. 28, Xi'an, Shaanxi 710049, People's Republic of China
[2] Department of Bioengineering and Beckman Institute for Advanced Science and Technology, University of Illinois at Urbana-Champaign, Urbana, IL 61801, USA
[3] Department of Physiology and Biomedical Engineering, Mayo Clinic College of Medicine, Rochester, MN, USA

E-mail: claramei@mail.xjtu.edu.cn, yuewang3@illinois.edu, fatemi.mostafa@mayo.edu and mfi@illinois.edu

Received 24 May 2016, revised 7 December 2016
Accepted for publication 21 December 2016
Published 17 January 2017

Abstract

Kelvin–Voigt fractional derivative (KVFD) model parameters have been used to describe viscoelastic properties of soft tissues. However, translating model parameters into a concise set of intrinsic mechanical properties related to tissue composition and structure remains challenging. This paper begins by exploring these relationships using a biphasic emulsion materials with known composition. Mechanical properties are measured by analyzing data from two indentation techniques—ramp-stress relaxation and load-unload hysteresis tests. Material composition is predictably correlated with viscoelastic model parameters. Model parameters estimated from the tests reveal that elastic modulus E_0 closely approximates the shear modulus for pure gelatin. Fractional-order parameter α and time constant τ vary monotonically with the volume fraction of the material's fluid component. α characterizes medium fluidity and the rate of energy dissipation, and τ is a viscous time constant. Numerical simulations suggest that the viscous coefficient η is proportional to the energy lost during quasi-static force-displacement cycles, E_A. The slope of E_A versus η is determined by α and the applied indentation ramp time T_r. Experimental measurements from phantom and *ex vivo* liver data show close agreement with theoretical predictions of the $\eta - E_A$ relation. The relative error is less than 20% for emulsions 22% for liver. We find that KVFD model parameters form a concise features space for biphasic medium characterization that described time-varying mechanical properties.

Keywords: *ex vivo* liver, gelatin emulsions, indentation, KVFD, viscoelastic modeling

(Some figures may appear in colour only in the online journal)

[4] The experimental work was carried out at the Beckman Institute for Advanced Science and Technology, University of Illinois at Urbana-Champaign, Urbana, IL 61801, USA. Methodological development, including numerical simulation and all data analysis, were carried out at the school of Life Science and Technology, Xi'an JiaoTong University, 710049, China.

1. Introduction

Mechanical properties of soft biological tissues have been studied extensively with the hope of enriching our collective understanding of how tissue composition and structure influence the mechanical properties that guide cellular behavior [1–5]. Tissue deformation patterns resulting from applied force stimuli can reveal properties of the tissue mechano-environment that influence cellular decision making in health and disease [6]. To exploit the diagnostic potential of this information, we must identify combinations of measurement techniques and data-reduction models that provide consistent parametric estimates corresponding to intrinsic tissue properties.

Deformation modeling is challenging because tissues are not material continua. Parameters derived from classical material modeling that represent mechanical measurements in tissues at one scale may not at another. Tissue properties are determined in part by fluid movement in the open- and closed-cell compartments found within a viscoelastic collagen matrix that is actively maintained by the embedded cells to meet programmed needs. These biphasic (solid/fluid) media exhibit multifaceted deformation responses that are particularly difficult to model using a concise feature set. Among the many techniques available for measuring mechanical properties, indentation testing remains the simplest and most recognized, and therefore has become the focus of our study. Time-dependent testing methods involving quasi-static loading yield force-relaxation curves and load-unload hysteresis loops that can reveal the intrinsic properties we seek.

It is common to parameterize time-varying mechanical responses using constitutive models that fit to measurement data [7]. Hookean elastic springs and Newtonian viscous dashpots are combined to parameterize the biphasic characteristics of soft tissues. Spring constants represent the elastic responses of connective-tissue elements and dashpot coefficients quantify viscous responses, each selected to summarize tissue components at a relevant scale and load rate. The ideal constitutive model for this purpose is able to represent more than one testing measurement over a practical range of medium properties and deformation rates with one set of parameter values. We aim to achieve consistently accurate models with as few parameters as possible to avoid overfitting. Such models are diagnostically useful if the parameters can be related to tissue components involved in disease processes. There is little evidence for such consistency with classic integer-order derivative models (Kevin–Voigt, Maxwell, and standard linear solid (SLS)) despite widespread use [8–10]. Some labs have shown that fractional-derivative models [11] can represent a range of measurement data with a small number of parameters [12–19]. Achieving the same close fit between models and measurement data using a Prony series and compound integer-order derivative models requires many more parameters [20].

The KVFD model has been applied to data from a wide range of multiphasic viscoelastic composite materials under different loading conditions [38–41]. We examined KVFD models applied to measurements of breast tissues following quasi-static uniaxial plate compressions in search of diagnostic indicators [38]. Others interpreted model parameters from data fit to compressed clays subjected to vertical-line loads to inform civil engineering applications [39]. Some general interpretation of medium composition and structure may be represented by model-parameter values, but these parameters are not intrinsic to the medium as they are also influenced by changing experimental conditions [21, 40]. KVFD model parameters describe how the microscopic properties of molecular crosslinking and fluid movement influence macroscopic properties like stiffness and mechano-biological state [41].

We previously examined the data-fitting accuracy of ramp-relaxation indentation measurements acquired from viscoelastic media using a Kelvin–Voigt fractional derivative (KVFD) model [21]. The aim of this report is to continue exploring that measurement-analysis combination by comparing different indentation-based measurement techniques applied to biphasic hydrogel emulsions and tissues. In this way, we can systematically relate changes in medium composition to variations in KVFD model parameters. Our analysis of the emulsions is then expanded to include measurements of *ex vivo* liver-tissue samples, some of which are heated to denature the collagenous matrix thus systematically modifying the mechanical properties. Together, the results suggest there is an interpretation of composite-medium properties in terms of model parameters that further encourages use of KVFD modeling in isotropic biological tissues.

2. Material and methods

2.1. Material preparation

2.1.1. Hydrogel samples. Emulsion samples included in these experiments were made from a combination of gelatin powder, deionized water, and a commercial skin cream, each component in precise weight concentrations. Gelatin powder (Type B gelatin, Rousselot, Dubuque, IA) was first mixed with deionized water in a beaker at room temperature and heated at 70 °C in a water basin for 45 min. The beaker was covered by aluminum foil during heating to minimize water evaporation. The mixture was stirred with a spoon every 5 min. Once the molten gelatin was removed from the water bath, it was cooled at room temperature to 30 °C while being periodically stirred. Then a mass of Vanicream (oil-in-water emulsion with oil-droplet size 100–1000 nm, Pharmaceutical Specialties, Inc., Rochester MN) was added to the clear gelatin and rapidly stirred for several minutes until a visually homogeneous milky-white liquid formed. The still-molten mixture was poured into cylindrical molds, sealed in plastic wrap, and stored at room temperature for 24 h to congeal before mechanical testing. Rigid plastic molds used to form the samples were cylindrical in shape, being 50 mm in diameter and 20 mm in height. It is essential that the manufacturing process be exactly reproduced in every detail if the mechanical properties of the samples are to be highly reproducible.

The congealed gelatin-cream samples are emulsions of cream particles suspended within the denatured collagen-

polymer aggregates, where cream particles on the order of 10 μm diameter are themselves a finer-scale oil-in-water emulsion. Fixing the gelatin concentration, the concentration of cream was increased as the water concentration decreased so the total sample mass remained constant. This recipe was scaled in volume to produce 6 samples at every cream concentration studied. As long as the gelatin concentration was held fixed, we will show that sample stiffness remains roughly constant. Cream adds a viscous-fluid component that generates a time-varying mechanical response during quasi-static compressive macro-indentation. Without cream, pure gelatin responds elastically [22].

A range of time-varying mechanical responses to indentation, similar to those observed in soft parenchymal tissues, was generated by varying both gelatin and cream concentrations as follows. At each of three gelatin concentrations (3%, 5%, and 8% by weight), we constructed 6 samples at one of five different cream concentrations (0%, 5%, 20%, 30%, and 50% by weight). Samples labeled G3C5 contain 3 g gelatin, 5 g Vanicream, and 92 g deionized water per 100 g of sample material. A sample labeled G8C20 has 8 g of gelatin powder, 20 g of cream, and 72 g of water per 100 g. From magnified visual inspection of the samples, it appears that cream particles in the congealed gel samples are liquid at room temperature (22 °C) where measurements are made.

2.1.2. Porcine liver. Frozen pig livers were obtained from a local market and completely thawed in water over several hours. Measurements were made on *ex vivo* liver samples at room temperature within 6 h of thawing. Samples roughly $40 \times 30 \times 15$ mm^3 in size were cut from liver lobes lacking major vasculature or ducts. Some specimens were tested without further processing. Others were tested after being heated in isotonic saline at 45 °C, 55 °C, or 65 °C for 40 min. After heating, samples were placed in new isotonic saline at room temperature for at least 45 min before indentation. Further experimental details are provided in section 3.4.

2.2. Methods

2.2.1. Indentation testing. Mechanical tests were conducted on all samples using the TA-XT Plus Texture Analyzer (TextureTechnologies,Algonquin,ILUSA)witha5mm-diameter spherical stainless steel indention probe. Two mechanical tests were performed on each sample: a ramp load-unload hysteresis test and a force-relaxation test with ramp-and-hold loading [23]. Time series and P-s curves for the two experiments are illustrated in figure 1. All hydrogel samples were tested while bonded to their cylindrical molds. The mold size was shown to be large enough to avoid significant boundary influences during indentation for pure gelatin samples at concentrations between 3% and 8% [24]. Liver specimens were tested when placed on a flat surface without constraining sample boundaries.

During ramp-hold force-relaxation testing (figure 1(a)), the maximum indentation depth was $s_{\max} = 1$ mm applied at the center of the cylindrical sample face. The ramp speed (probe velocity) was $v = 0.04$ mm s^{-1} delivered during a ramp time of $T_r = 25$ s. Subsequently, probe position was held constant for 300 s as relaxation of the force was monitored. The same experimental parameters ν and T_r were applied during load-unload testing, where ramp-load (P_1-s) and ramp-unload (P_2-s) curves were recorded (figure 1(b)).

In both tests, deionized water was added to the top surface of the samples so the spherical indenter was submerged. We showed this method reduces probe-sample adhesion forces to negligible values. We also verified that the water was not significantly absorbed by the samples during the measurement time [24].

2.2.2. Kelvin–Voigt fractional derivative (KVFD) model. Others [12, 13] have shown the KVFD model is an accurate and flexible method for generating a concise set of parameters describing the mechanical responses of biphasic media during quasi-static deformation.

The constitutive equation relating stress $\sigma(t)$ to strain $\varepsilon(t)$ for the fractional-derivative Kelvin–Voigt model is expressed as [14, 15]

$$\sigma(t) = E_0\varepsilon(t) + \eta\frac{\mathrm{d}^\alpha\varepsilon(t)}{\mathrm{d}t^\alpha}, \tag{1}$$

where E_0 is an elastic modulus (Pa), $\eta = E_0\tau^\alpha$ is a viscous coefficient (Pa-s^α) with time constant $\tau(s)$, and α is a unitless real number between (0, 1) that defines the derivative order. A primary goal of this paper is to relate model parameters E_0, α, τ to changes in gelatin and cream concentrations, while controlling for experimental parameters v, T_r, as we test whether measurements of model parameters can be used to identify medium components.

Relaxation modulus G is defined through the Boltzmann superposition equation [14, 15]

$$\sigma(t) = \int_0^t G(t-\tau)\frac{\mathrm{d}\varepsilon(\tau)}{\mathrm{d}\tau}\mathrm{d}\tau. \tag{2}$$

Equating the Laplace transforms of equations (1) and (2), solving for G, and transforming back to the time domain yields the relaxation modulus for the KVFD model in two forms,

$$G(t) = E_0\left(1 + \frac{(t/\tau)^{-\alpha}}{\Gamma(1-\alpha)}\right) = E_0 + \eta\left(\frac{t^{-\alpha}}{\Gamma(1-\alpha)}\right), \tag{3}$$

where $\Gamma(\cdot)$ is a gamma function (see equation (7)). For the spherical indenter geometry, it was shown [14–16] that time-varying force $P(t)$ and displacement $s(t)$ could be substituted for stress and strain in equation (2) to give

$$P(t) = \frac{8\sqrt{R}}{3}\int_0^t G(t-\tau)\frac{\mathrm{d}s^{3/2}(\tau)}{\mathrm{d}\tau}\mathrm{d}\tau \tag{4}$$

where $s(t)$ is specifically the depth of the indenter tip into the surface relative to the uncompressed equilibrium state of the sample surface.

2.2.3. Ramp-hold force relaxation experiment. The measured relaxation force can be modeled as a function of time-varying displacement $s(t)$ and three KVFD model parameters descriptive of the compressed medium,

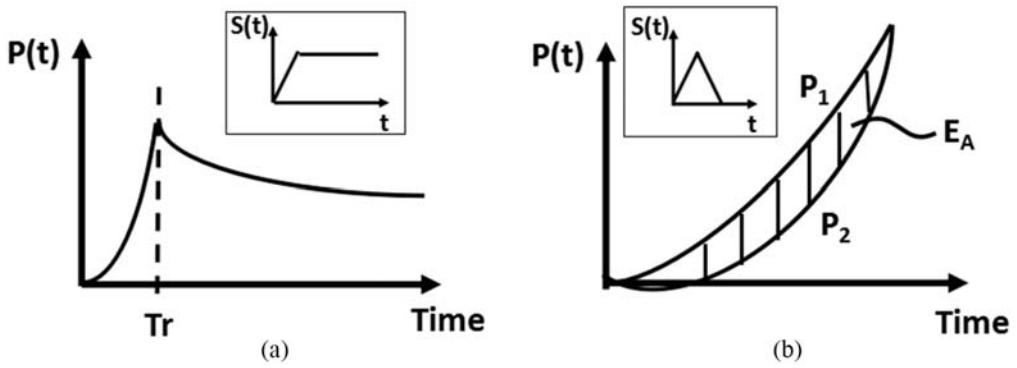

Figure 1. Response curves for the (a) ramp-hold relaxation and (b) load-unload indentation experiments are diagrammed. P is the measured force, s is the indentation depth, T_r is the ramp time over which the probe tip is displaced at constant velocity into the sample surface to reach a 1 mm depth, and E_A is the loss-energy estimate found from the area between the load-unload curves in (b) once probe-sample adhesions are eliminated.

$$P(t) = f(t, s(t), E_0, \alpha, \tau). \tag{5}$$

Given the ramp-hold displacement function,

$$s(t) = \begin{cases} vt, & 0 \leqslant t \leqslant T_r \\ s_{max} = vT_r, & t \geqslant T_r \end{cases}, \tag{6}$$

the ramp-hold relaxation force resulting from spherical indentation can be expressed by [21],

$$P(t) = \begin{cases} 4\sqrt{R}\, s^{\frac{3}{2}} E_0 \left[\frac{2}{3} + \frac{(t/\tau)^{-\alpha}}{\Gamma(1-\alpha)} B\left(\frac{3}{2}, 1-\alpha\right) \right], & 0 < t \leqslant T_r \\ 4\sqrt{R}\, s_{max}^{\frac{3}{2}} E_0 \left[\frac{2}{3} + \frac{\left(\frac{t}{T_r}\right)^{\frac{3}{2}} \left(\frac{t}{\tau}\right)^{-\alpha}}{\Gamma(1-\alpha)} B\left(\frac{T_r}{t}; \frac{3}{2}, 1-\alpha\right) \right], & t \geqslant T_r \end{cases} \tag{7}$$

where $\Gamma(z) = \int_0^\infty e^{-t} t^{z-1} dt$ is a Gamma function, $B(x, y) = \int_0^1 t^{x-1}(1-t)^{y-1} dt \quad \mathrm{Re}(x) > 0, \mathrm{Re}(y) > 0$ is a beta function, and $B(a; x, y) = \int_0^a t^{x-1}(1-t)^{y-1} dt \quad a \in [0, 1]$ is an incomplete beta function.

The three KVFD model parameters are estimated simultaneously by fitting the ramp solution in equation (7) to force-relaxation measurement data [21].

2.2.4. Loss-energy measurements from load-unload hysteresis experiment. When media are subjected to cyclic ramp loading-unloading and found to respond differently for the load phase than the unload phase, the area between the P-s curves (figure 1(b)) is the loss energy E_A,

$$E_A = \int_0^{T_r} ds(P_1(s) - P_2(s)). \tag{8}$$

E_A is the energy dissipated in the sample over time due to internal frictional losses provided that adhesions between the probe and sample surfaces are made negligible [17].

2.2.5. Predicting loss-energy measurements E_A. The displacement during each load-unload cycle is a triangular function of time,

$$s(t) = \begin{cases} vt, & 0 \leqslant t \leqslant T_r \\ v(2T_r - t), & T_r \leqslant t \leqslant 2T_r \end{cases}. \tag{9}$$

From equations (4) and (8),

$$E_A = \int_0^{T_r} ds(t)(P_1(t) - P_2(2T_r - t)), \tag{10}$$

$$\text{where} \begin{cases} P_1(t) = 4\sqrt{R}\, v^{3/2} \int_0^t G(t-\tau)\tau^{1/2} d\tau, & 0 < t \leqslant T_r \\ P_2(t) = 4\sqrt{R}\, v^{3/2} \left[\int_0^{T_r} G(t-\tau)\tau^{1/2} d\tau \right. & T_r \leqslant t \leqslant 2T_r. \\ \quad \left. - \int_{T_r}^t G(t-\tau)(2T_r - \tau)^{1/2} d\tau \right] \end{cases} \tag{11}$$

Since there is no closed-form analytic solution for equation (10), E_A is calculated by numerical integration. In the results section, we explore the relationship between E_A and η under different combinations of model parameters for fixed ramp speed v, to discover any relationships between the two quantities.

2.2.6. Statistical analysis. The elastic modulus of these samples is very sensitive not only to component materials but to the thermal history of the gelatin gel during manufacturing and storage. We occasionally made all 6 samples on 1 d and at other times 2 samples each day over 3 d. In this way, inter-sample variability was observed as well as measurement uncertainty. Error bars in plots summarizing gel-cream sample measurements are standard deviations of one measurement from each of 6 samples, unless otherwise noted. Error bars for liver-tissue measurement data are standard deviations of three measurements made on one liver sample acquired at different locations (we assumed liver tissue and gel samples were isotropic).

In section 3.3, we display *measurements* of energy loss denoted by $\widehat{E_A}$ to distinguish them from *predictions* E_A made via equation (10). To evaluate confidence intervals between measured and predicted values, we computed a relative error using

$$e_{\mathrm{r}} = \frac{\left|\widehat{E}_A - E_A\right|}{E_A}. \tag{12}$$

An analysis of variance (ANOVA) method was applied to analyze the sensitivity of each measured KVFD parameter to sample component concentrations. Two-way ANOVA was applied to examine the influence of two component variables, viz., gelatin percentage and cream percentage, on each KVFD parameter measured from a ramp-relaxation test. We rejected the null hypothesis when $p < 0.05$.

3. Results

3.1. KVFD modeling of measurement data

Ramp-relaxation measurements for each gel-cream emulsion sample were combined in a regression fit with equation (7) to estimate KVFD model parameters E_0, α, and τ for that sample. To illustrate, the best-fit model response (line) for sample G5C20 is shown along with the measurement data (dots) in figure 2(a). Applying the same parameter estimates (without further fitting) to equation (10), the predicted force response (line) in figure 2(b) is compared with load-unload hysteresis measurements (dots). Hence KVFD model parameters estimated from data obtained using the ramp-hold experiment closely predict data obtained from a load-unload hysteresis experiment except over those times when the probe separates from the sample.

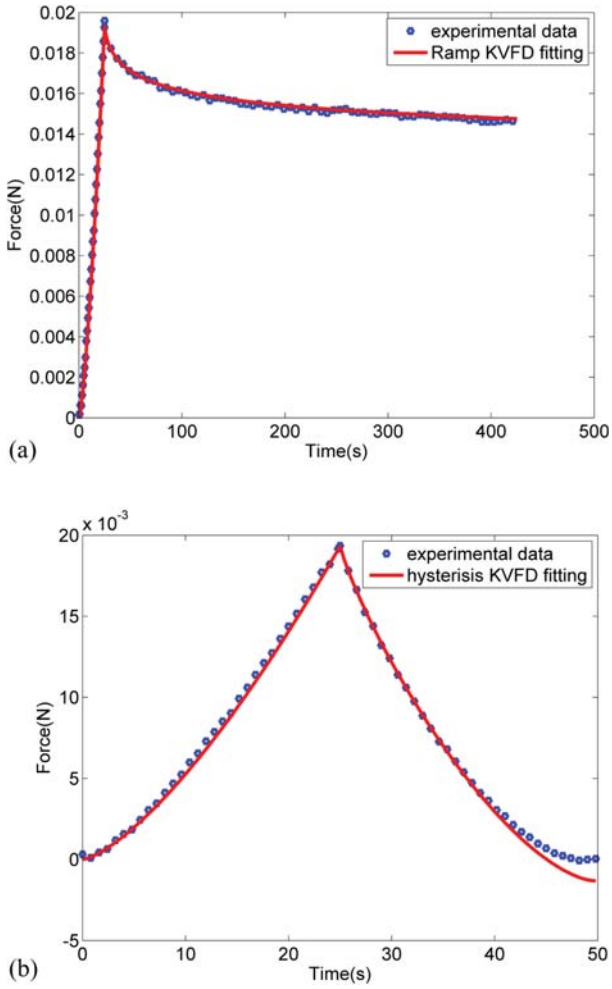

Figure 2. Model fitting for ramp-relaxation (a) and load-unload experimental data (b). (a) Fitting equation (7) (solid line) to the ramp-relaxation data (dots) acquired from a G5C20 sample, we found the KVFD model parameters $E_0 = 2.38$ kPa, $\alpha = 0.16$, and $\tau = 8.31$ s. (b) Applying those same parameter values to equation (10) we predicted force $P(t)$ for the load-unload experiment that closely represents the measurements (dots). The disagreement near $t = 50$ s is most likely caused by the model not predicting the experimental observation in which the probe separates from the sample surface.

3.2. Interpreting KVFD model parameters for ramp-relaxation data

Physical interpretations of E_0, α, and τ begin with their definitions in equations (1)–(3). In the following sections we amplify upon those interpretations for the media in this study using measurement data features. E_0 is the relaxation modulus measured at infinite time, $E_0 = G(\infty)$. The fractional-order parameter $0 < \alpha < 1$ is widely regarded as a measure of material fluidity; specifically, $\alpha \to 0$ for solids and $\alpha \to 1$ for fluids. Intermediate values of α reflect mixtures of the two phases [18, 19]. Relaxation time constant τ scales measurement time t in the factor $(t/\tau)^{-\alpha}$ of equation (3). It combines with α to give the initial medium response to ramp loading.

3.2.1. Elastic parameter E_0. The elastic modulus measured by applications of the Kevin–Voigt (integer-order derivative) model approximates the shear modulus [24, 25]. To show this is also true for the KVFD model, we compared E_0 in equation (3) with the elastic modulus determined from Hertzian contact theory and wave-propagation measurements. Since the latter quantities only apply to linear-elastic solids, measurements in pure-gelatin cylinders were acquired for these comparisons; viz., samples G3C0, G5C0, and G8C0. We estimated shear modulus via Hertzian theory by assuming gelatin gels are incompressible. In that case, Hertzian estimates of Young's modulus are divided by three to estimate the shear modulus.

Table 1 shows that values for KVFD parameter E_0 approximate the shear modulus when one set of force-displacement data are analyzed both ways. The table also shows the results approximate those using other measurement techniques [24–26].

Estimates of E_0 for all emulsion samples are summarized in figure 3(a). Each curve displays data at a different gelatin concentration as a function of cream concentration. Clearly, E_0 increases with gelatin concentration. E_0 also increases with cream concentration initially from changes to the crosslinking structure of the denatured collagen aggregates as cream particles are introduced. At higher cream concentrations, however, sample stiffness is relatively insensitive to

Table 1. Comparison of E_0 and shear modulus values from gelatin gel samples.

Gelatin % (sample label)	KVFD E_0 (Pa)	Hertzian Shear modulus (Pa)	Shear modulus[b] (Pa)
3% (G3C0)	329 ± 11	292 ± 14	$320 \pm 28^{**}$
5% (G5C0)	766 ± 30	806 ± 18	930[a]
8% (G8C0)	2120 ± 80	2070 ± 27	$2286 \pm 315^{***}$

[a] Measurements from [24] in pure gelatin at concentrations of 2%, 4%, 6%, and 8% were fit to the polynomial $y = 178.75x^2 - 426.5x + 485$ to interpolate and estimate a value at 5%. Thus no error bar is reported. Orescanin *et al* reported gelatin prepared in the manner of our study by applying an ultrasonic impulse-response measurement method to 3% gelatin** [25] and rheometer-based estimates to 8% gelatin*** [26].
[b] Comparisons are with previous measurements made in our lab to minimize sample-preparation variability.

cream concentrations[5]. Two-way ANOVA test results showed significant differences between various gelatin concentrations ($p = 0.0005$) and less significant differences between various cream concentrations ($p = 0.129$).

In summary, KVFD model parameter E_0 approximates the shear modulus of the sample that is determined primarily by gelatin concentration. It describes the stiffness of the denatured collagen aggregates that form the solid matrix within these biphasic samples. As shown in figure 3(b), E_0 mainly acts to scale $P(t)$, thus reflecting the elastic response in the ramp relaxation curve that is relatively insensitive to cream at concentrations between 20% and 50%.

3.2.2. Derivative-order parameter α. The data in figure 3(c) show that α increases linearly with cream concentration. Because points overlap, we also see that α is independent of gelatin concentration. Two-way ANOVA tests confirm there are no significant differences between gelatin concentrations ($p = 0.82$).

A linear increase of α with cream percentage is consistent with that parameter being related to sample fluidity. Moreover, parameter α also characterizes the rate of energy dissipation with time. As shown in figure 3(d), α determines both the peak force and the shape of the force-relaxation curve during ramp-hold indentation tests. Larger α values correspond to more fluid samples, which generates a smaller force peak. Then the applied energy dissipates quickly as the force returns to equilibrium. One expects such behavior in highly fluidic biphasic media with large α because of the weak elastic response. Smaller values of α generate higher force peaks and the energy dissipates more slowly. This is expected from a viscoelastic matrix embedded in some fluid. Relaxation of a viscoelastic solid depends on the degree and type of molecular bonds in the matrix connections [19, 28]. The extracellular matrix in tissues and the matrix in these emulsion samples have very different collagen-component structures, and yet both naturally self-assemble in fluids to respond viscoelastically. In such media, we generally find that $\alpha > 0.2$ [19]. In contrast, pure gelatin has tightly bound water that strongly adheres to exposed charged sites in the denatured collagen molecules, so it responds as an elastic solid [28, 29]. For pure gelatin we find $\alpha \approx 0$. Our findings are consistent with those of others studying wet clay [40].

3.2.3. Time constant τ and viscous coefficient η The first form of equation (3) shows that α and τ combine with measurement time t to predict the rate at which the indentation force relaxes through the power-law factor $(t/\tau)^{-\alpha}$. The second form of equation (3) combines terms in the expression $\eta = E_0\tau^{\alpha}$, where η is the viscous coefficient for the time-dependent component of the relaxation modulus G.

Figure 4(a) shows that τ increases with cream concentration but not gelatin concentration. This finding shows an increase in viscous relaxation for the solid matrix of the emulsion. For a given α, parameter τ characterizes the recovery speed of the relaxation process to its equilibrium state. Larger τ values correspond to slower recoveries. Higher cream concentrations increase the viscosity and require longer recovery times.

Measurements of the viscous coefficient in figure 4(b) show that η increases with both cream and gelatin concentrations. However, normalizing the viscous coefficient by the elastic modulus, i.e. η/E_0, we can eliminate the gelatin-concentration dependence as shown in figure 4(c). This result indicates that parameters α and τ together determine the time-dependent viscous behavior and are related to the energy loss in the emulsion. Finally, figure 4(d) shows the ramp-relaxation curves predicted for different values of τ.

3.3. Interpreting KVFD model parameters for load-unload data

Ramp-relaxation indentation was applied to samples in the last section. This section examines load-unload indentation testing so we may measure the loss energy E_A from the load-unload hysteresis curve (figure 1(b)). The goal is to relate the KVFD parameters estimated from ramp-relaxation data to E_A measured from load-unload data.

Numerical simulations were first performed to examine possible correlations between the viscous coefficient η and loss energy E_A. Predictions were made for all combinations of the three KVFD parameters: E_0 was varied from 0.1 to 7.3 kPa, α from 0.01 to 0.7, and τ from 0.1 to 2500 s. These parameter ranges span those observed experimentally in the emulsions and liver-tissue samples (described below).

The simulation results in figure 5(a) show that loss energy E_A is proportional to the KVFD viscous coefficient η, i.e. $E_A = k\eta$, where the proportionality constant k depends on material parameter α and experimental parameter T_r, viz., $k = k(\alpha, T_r)$. Fixing $T_r = 25$ s, each line in figure 5(a) is associated with a different value of α. That is, combinations of E_0 and τ for fixed values of α and T_r can be found along the straight lines. Proportionality between E_A and η suggests that energy loss in a load-unload indentation experiment, which

[5] There are well-known secondary effects in gelatin that contribute to variations in E_0 with cream concentration. For example, Vanicream is acidic (pH = 3.73). Increasing gelatin acidity during the gelation process will soften the samples [27]. Thus the downward trend in E_0 at cream concentrations observed above 20% is expected.

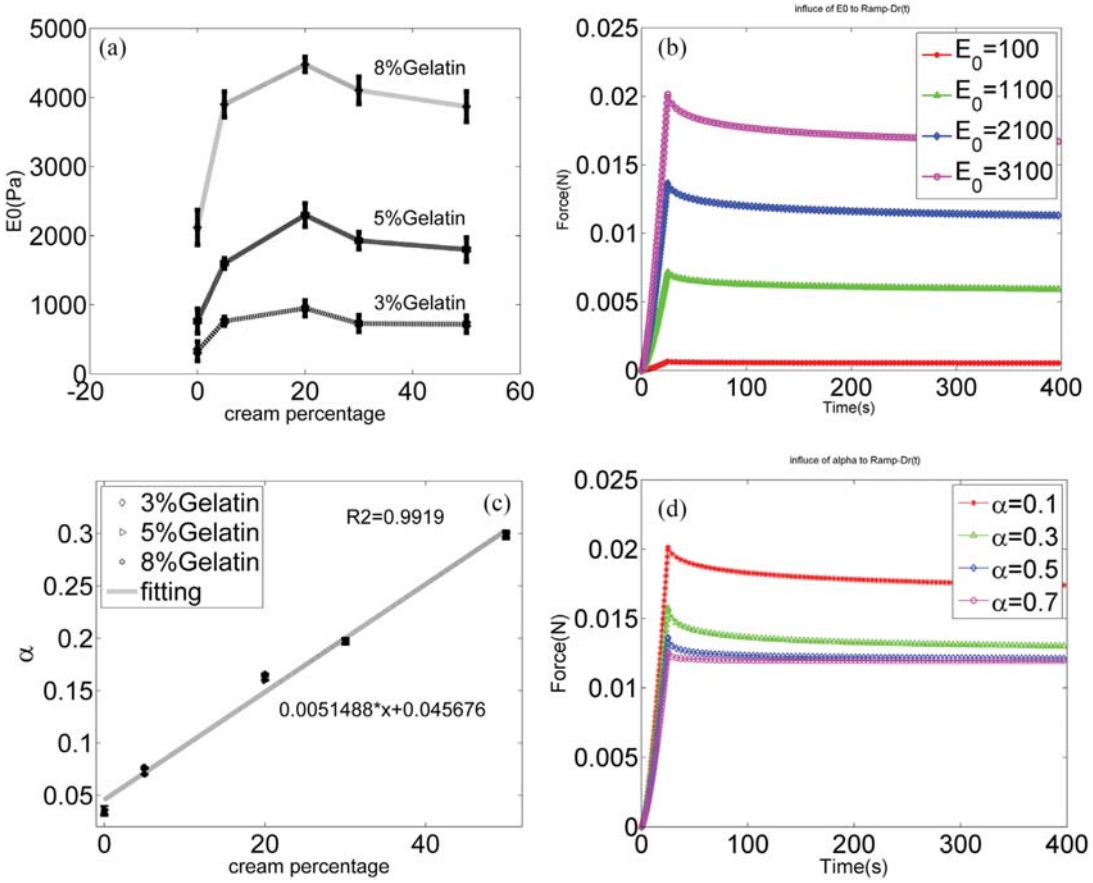

Figure 3. (a) Measurements of KVFD parameter E_0. (b) Ramp-relaxation curves are modeled for different values of E_0 assuming fixed values $\alpha = 0.16$ and $\tau = 8.3$ s. (c) The linear dependence of α on sample cream concentrations is shown. The line labeled 'fitting' is found from a linear regression of all of the data shown ($R^2 = 0.992$). The small error bars indicate ± 1 s.d. obtained from measurements on six samples. (d) Ramp-relaxation curves predicted for different values of α for fixed $E_0 = 2.83$ kPa and $\tau = 8.3$ s. Note the peak value at $t = T_r = 25$ s and the relaxation rate both change with α.

is a model-independent quantity, is highly correlated to η the viscous coefficient in a ramp-hold experiment.

Figure 5(b) displays E_A versus α for η fixed at 800 Pa-s$^\alpha$ and at four values of T_r. E_A peaks at a different value of α for each ramp time. The presence of a peak in these curves can be explained physically. As $\alpha \to 0$, we find that $E_A \approx 0$ indicating an elastic medium that exhibits little frictional loss. Similarly, as $\alpha \to 1$, we again find $E_A \approx 0$ but now indicating a fluid medium under a quasi-static load. Fluid-medium energy loss is smallest for the slowest ramp speed ($T_r = 100$ s). In between these extremes, viscous response of the collagen matrix within the emulsion is magnified by distributed pockets of fluid exhibiting high internal friction. Energy dissipation is greatest at the highest ramp speed, $T_r = 10$ s.

Those simulations were verified experimentally in figure 6. Measurements of E_A (points) for emulsion samples that were acquired during load-unload experiments are plotted against separate measurements of η for the same samples obtained from ramp-relaxation experiments. Lines associated with measurement points in the figure are predictions made using equation (10) for the average α measurement. Each line corresponds to the averaged α value of certain cream percentage ($\alpha = 0.035$, 0.07, 0.16, 0.197, 0.3 for cream percentage 0%, 5%, 20%, 30%, 50%). As predicted, measurements from samples with the same cream concentration have approximately the same α values. In contrast, samples with different gelatin concentrations fall along a straight line determined by α in the η versus E_A plane. Predictions were verified by emulsion measurements where each sample had one of the following cream percentages: 0%, 5%, 20%, 30%, and 50%. Results show that the measured loss energy from quasi-static load-unload experiments is linearly related to the viscous coefficient computed from the KVFD model applied to ramp-relaxation experiments. One set of model parameters describes data from both experiments. Hence, the KVFD parameters apply equally well to the data from these different indentation techniques.

Fractional bias error is $e_b = \left|\widehat{E}_A - k_\alpha \overline{\eta}\right| / k_\alpha \overline{\eta}$ as shown in the figure, where $\overline{\eta}$ is the mean value. In brackets we display confidence interval $e_a, e_c = \left|\widehat{E}_A - k_\alpha(\overline{\eta} \pm \sigma)\right| / k_\alpha(\overline{\eta} \pm \sigma)$ predicting the error range associated with σ, which is the standard deviation for η estimates. For example, the numerator for error e_c is illustrated in the figure below.

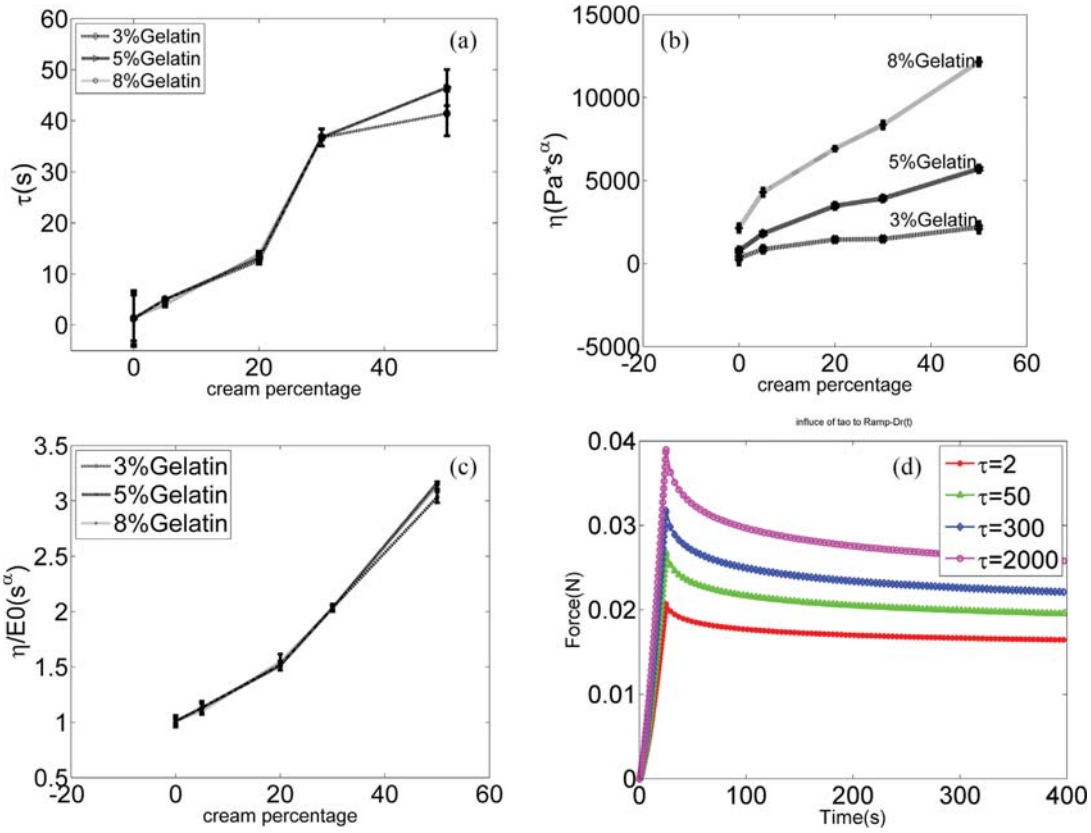

Figure 4. (a) The monotonic increase in KVFD parameter τ with cream concentration is essentially independent of gelatin concentration. (b) However, the increase in viscous coefficient η with cream concentration does depend on gelatin concentration unless η is normalized by E_0, as shown in (c). Error bars shown indicate ± 1 s.d. for measurements on six samples. (d) Ramp-relaxation curves predicted for different values of τ are shown when we fix $E_0 = 2.83$ kPa and $\alpha = 0.16$.

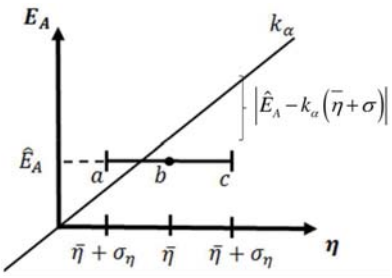

Table 2 shows the relative uncertainties in E_A predictions given errors in η measurements. Table values are bias errors; the two values in brackets below give the confidence intervals corresponding to ± 1 standard deviation for each η measurement. All bias errors are less than 20% and many are less than 5%; the notable exception being the elastic, 0% cream samples. Stiff elastic samples generate the largest prediction errors.

The magnitudes of the relative errors and confidence intervals indicate that it is reasonable to use a pre-generated prediction plot to relate loss energy and viscous coefficient parameters in our test samples. Consequently, either measurement can be made to estimate KVFD parameters.

In summary, KVFD model parameters, E_0, α, and τ, characterize, respectively, the elasticity, the fluidity and the rate of energy dissipation, and the viscous time constant of compressed biphasic emulsions. These model parameters help explain the response of samples to indentation in terms of sample components and molecular structure. E_0 is the shear modulus that quantifies material stiffness controlled primarily by gelatin concentration. Within the cream-concentration range of 20–50%, emulsion stiffness does not significantly change, although secondary effects provide small systematic variations. Parameter α indicates the rate at which the emulsion internally dissipates mechanical energy. In this study, it increases in proportion to the replacement of water with cream.

We find that two parameters, E_0 and $\eta/E_0 = \tau^\alpha$, form a representative feature space that describes, respectively, the stiffness and the normalized viscosity of the emulsions. In addition, E_0 increases predictably with gelatin concentration, independent of cream concentration, while the ratio η/E_0, the normalized viscous coefficient, increases predictably with cream concentration and is independent of gelatin concentration. Further, η measured using ramp-relaxation testing is proportional to loss energy E_A measured from the hysteresis in load-unload experimental curves.

3.4. Liver samples

We now extend our analysis of KVFD model parameters to *ex vivo* liver tissue. Of course, liver is compositionally and

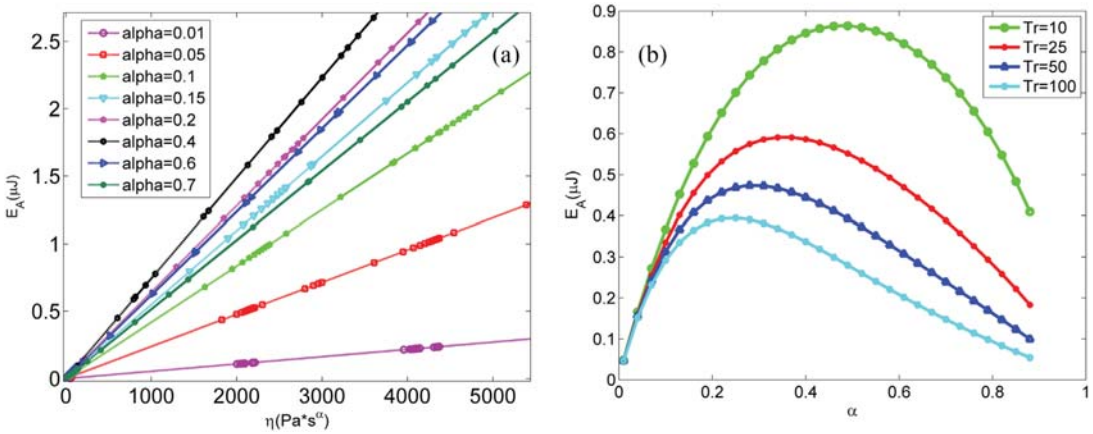

Figure 5. (a) Predicted relationships between viscous coefficient η and loss energy E_A are illustrated for eight values of α between 0 and 1, all at $T_\tau = 25$ s. (b) E_A is plotted as a function of α for four ramp-time values T_τ each for a fixed value of $\eta = 800$ Pa-s$^\alpha$. The maximum indentation depth is fixed at $s_{max} = 1$ mm.

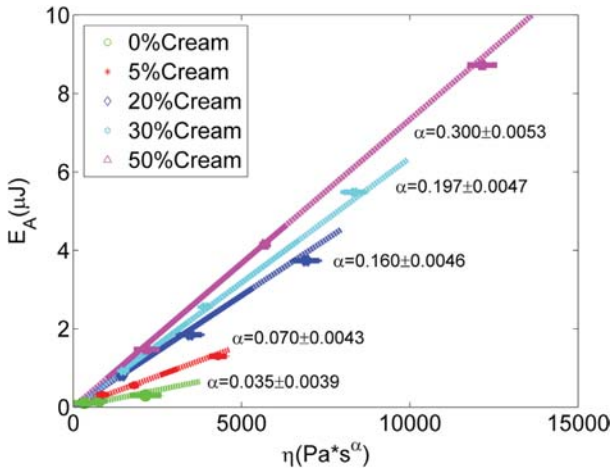

Figure 6. The predictions of figure 5 (lines) are compared with measurements on emulsion samples (points). Three gelatin concentrations, 3%, 5%, and 8%, at each of the five cream concentrations indicated in the legend are shown. A fixed cream concentration establishes a line corresponding to α, along which we find the three gelatin concentrations. Along each line, the 3% gelatin samples have the smallest E_A value while the 8% gelatin samples have the largest. Error bars indicate ± 1 s.d. for samples as described in table 2.

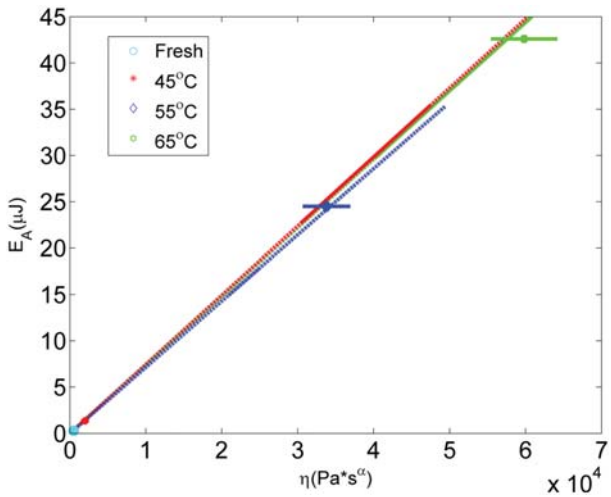

Figure 7. Similar to figure 6, we plot measurements of E_A versus η for *ex vivo* liver samples. The cyan circle marker near the origin is the result for liver that was not heated (labeled fresh). The red star marker also near the origin indicates results for liver heated to 45 °C for 40 min. The blue diamond and green hexagram markers indicate measurements for liver heated for 40 min to 55 °C or 65 °C, respectively. Error bars along both axes indicate ± 1 s.d. in η and E_A measurements. The lines are for values of $\alpha = 0.41$, 0.35, 0.27, found from ramp-relaxation measurements where $T_\tau = 25$ s.

structurally more complicated than two-component gelatin-cream emulsions. Nevertheless, it is an important test medium for its well-known mechanical response to heating [30–34].

A major medical application of liver-tissue heating is curative nonsurgical treatments of hepatocellular carcinoma. Liver is locally heated in patients, *in vivo*, using percutaneous radiofrequency ablation, microwave ablation, or high-intensity ultrasound (HIFU) techniques [35, 36]. Heating liver to 45 °C for 30–60 min irreversibly damages cells, inhibiting DNA replication and mitochondrial function [36]. Fast heating to temperatures above 60 °C causes irreversible protein denaturation, which is also cytotoxic and leads to coagulative cellular necrosis. Besides the desired cellular damage, extracellular protein structure is altered in ways that can be sensed through macroscopic mechanical testing [32, 33].

We used a simple technique of heating porcine liver samples in isotonic saline. Frozen livers were thawed in room temperature saline overnight. Samples were then transferred to saline heated in a double boiler to 45 °C, 55 °C, or 65 °C for 40 min. Samples were then removed from the heated saline and cooled in room temperature saline for 45–60 min before testing began. Specimens were placed on a flat surface during testing without boundary constraints. Each sample size was roughly $40 \times 30 \times 15$ mm^3, large enough to avoid significant boundary effects during indentation.

Measurements of thermally-damaged liver are compared with those of fresh liver in figure 7 and table 3. Note that 'fresh' refers to samples that were not heated; all liver tissues were initially frozen. As with the emulsion samples, we

Table 2. Prediction errors and confidence intervals are given for samples with different gelatin concentrations (rows) and cream concentrations (columns). Errors for pure gelatin samples are found in the 0% column.

	0%	5%	20%	30%	50%
3%	0.156 [0.103 0.369]	0.177 [0.031 0.321]	0.019 [0.046 0.083]	0.025 [0.046 0.096]	0.149 [0.103 0.196]
5%	0.173 [0.123 0.464]	0.026 [0.054 0.106]	0.066 [0.038 0.094]	0.025 [0.003 0.054]	0.008 [0.018 0.035]
8%	0.199 [0.083 0.314]	0.044 [0.009 0.078]	0.051 [0.036 0.066]	0.033 [0.019 0.047]	0.033 [0.020 0.047]

Table 3. *Ex vivo* liver samples measurement. Note that shear-modulus values for liver are about 30 times less than typical literature values, e.g. [33].

	Fresh	Heated 45 °C	Heated 55 °C	Heated 65 °C
E_0 (Pa)	75 ± 11	188 ± 22	4150 ± 368	7398 ± 587
α	0.41 ± 0.01	0.35 ± 0.007	0.27 ± 0.005	0.27 ± 0.004
τ (s)	103 ± 12	850 ± 71	2300 ± 106	2500 ± 127
η ($\times 10^4$ Pa-s$^\alpha$)	0.050 ± 0.020	0.199 ± 0.051	3.38 ± 0.313	5.98 ± 0.437
E_A (μJ)	0.289 ± 0.033	1.36 ± 0.099	24.5 ± 0.98	42.6 ± 2.14
e_b [e_a, e_c]	0.224 [0.142, 0.382]	0.130 [0.092, 0.224]	0.023 [0.008, 0.015]	0.004 [0.003, 0.003]
η/E_0 (s$^\alpha$)	6.67 ± 1.27	10.59 ± 1.61	8.14 ± 1.46	8.08 ± 0.68

measured $\eta(E_0, \alpha, \tau)$ using ramp-relaxation experiments and fit those data to the KVFD model to estimate model parameters. We also measured E_A using load-unload experiments. $T_r = 25$ s was applied to all liver measurements. Mean estimates from the two experiments are plotted against each other in figure 7. The last line in Table 3 lists the bias errors and confidence intervals expected when predicting loss energy from KVFD parameters.

4. Discussion

Table 3 summarizes the *ex vivo* liver-tissue measurements obtained by fitting the KVFD model to ramp-relaxation and load-unload experimental data. Thermally damaged liver clearly exhibits modified parameters. Generally, liver heated to higher temperatures dramatically increases E_0 and τ while α decreases by about a third relative to tissue that was not heated. Other investigators [32–34, 36] reported that heating liver above 55–60 °C irreversible transforms Type 1 collagen in tissue stroma from its normal helical fiber state to one more randomly structured, and this structural change leads to increased stiffness (E_0) from additional collagen cross linking [34, 37]. The values shown in table 3 suggest the increase in η is due to the increase in E_0. That is, η/E_0 is not significantly modified by heating. Table 3 shows that thermally damaged liver becomes stiffer, more dissipative, and less fluidic but it maintains a relatively constant normalized viscous coefficient. All of these indicators, including the increase in loss energy with the degree of thermal damage, appear as primarily elastic-property changes caused by an increased density of cross links in thermally-damaged collagen.

The data in table 3 and figure 7 show that the *ex vivo* liver samples undamaged by heat have a strong fluidic response to indentation ($\alpha = 0.41$) and are soft ($E_0 = 75$ Pa) dissipating little mechanical energy ($E_A = 0.29$ μJ). These shear modulus estimates are smaller than most estimates reported in the literature for *in vivo* or freshly-excised liver [31]. Our values in table 3 are smaller for several reasons: (a) freezing tissue causes cell damage that softens tissues once thawed. (b) Longer ramp times applied to minimize the effects of instrument responses on the stress-relaxation data also lower modulus values compared to shorter ramp times [21]. (c) Submerging samples in saline reduces sample-to-sample variations but also reduces stiffness [43]. Although the overall elastic modulus of samples used in this study is lower than that reported *in vivo*, the relative response to tissue heating is similar. Table 3 shows that heating liver to 45 °C (and measuring at 22 °C) stiffens the tissue ($E_0 = 188$ Pa) as it creates a more solid ($\alpha = 0.35$) and dissipative ($E_A = 1.36$ μJ) medium.

Heating liver to 55 °C causes a major transformation in tissue structure, as noted by others [32, 33, 36]. We find that liver stiffness increases more than 20 fold ($E_0 = 4150$ Pa) compared to the value of E_0 at 45 °C. At 55 °C, the extracellular collagen denatures to expose charged sites that form a higher density of cross links. This process further solidifies the tissue ($\alpha = 0.27$) with viscoelastic cross links that greatly increases loss energy ($E_A = 24.5$ μJ). Parameter τ changes drastically at this temperature also, probably from the suddenly increased number of chemical bonds.

At 65 °C, liver stiffness increases further ($E_0 = 7398$ Pa) while α and τ change very little. Between 55 °C and 65 °C, loss energy doubles ($E_A = 42.6$ μJ), which can be attributed entirely to changes in E_0. Interestingly, figure 5(b) predicts that for the indentation ramp time of $T_r = 25$ s that we applied during liver measurements, we can expect there to be no significant change in loss energy E_A related to changes in α. The reason is that α values in liver for $T_r = 25$ s are near the peak of the α versus E_A curve. Consequently, loss energy is not expected to be sensitive to changes in tissue fluidity. Care must be taken to adjust experimental parameters appropriately to maximize KVFD parameter changes when the goal is to track thermal damage.

Changes observed in thermally-damaged *ex vivo* liver are likely to be different from those measured *in vivo*. The effects of blood perfusion, at the very least, modify the temperature

distribution in ablative therapy where tissue temperatures quickly rise above 80 °C and fall as blood perfusion cools the region. The rates of tissue heating and cooling will have additional effects on mechanical properties. Our point in this study is not to predict *in vivo* tissue effects. Instead, our goal is to show that KVFD model parameters can explain known basic effects of thermal damage in tissues as complex as liver.

5. Summary and conclusions

The KVFD model of the relaxation modulus summarized by equation (3) provides a 3D feature space of mechanical properties that characterizes the composition and structure of biphasic emulsions. We found that the combination of KVFD parameters given by E_0 and $\eta/E_0 = \tau^{\alpha}$ was able to separately track the compositional changes in the emulsions. Also these model parameters were found to equivalently apply to data from different indentation experiments. Based on our experience analyzing emulsion samples, we then studied indentation measurement data from *ex vivo* porcine liver samples. We found the KVFD model parameters described changes caused by thermal damage that were consistent with results found in the literature—increased H-bond cross linking from protein denaturation. From these combined results, we conclude that KVFD model parameters form a concise features space for biphasic medium characterization that described time-varying mechanical properties.

Experimental factors can influence the parameters obtained by fitting model equations to force-displacement indenter data. However these influences are consistent between different indentation method, and thus a concise feature set can be formed to reliably represent material properties. This is an important result for medical elasticity imaging, where images formed from KVFD parameters are interpreted for detecting disease processes or treatment-induced effects. KVFD model parameters are worthy of further study for medical imaging applications and as indicators for disease differentiation.

Acknowledgments

The authors gratefully acknowledge support in part from the National Cancer Institute of the US National Institutes of Health under award number ROI CA168575, The National Science Foundation ECCS-1306808, and the China Scholarship Council. The content is solely the responsibility of the authors and does not necessarily represent the official views of NIH or NSF. The authors gratefully acknowledge a generous supply of gelatin provided by Rousselot Inc., Dubuque IA. All experiments were carried out at the Beckman Institute for Advanced Science and Technology, University of Illinois at Urbana-Champaign, Urbana IL, 61801, USA. Numerical simulations and data analysis were carried out at the school of Life Science and Technology, Xi'an JiaoTong University, China.

References

[1] Hoyt K *et al* 2008 Tissue elasticity properties as biomarkers for prostate cancer *Cancer Biomarkers* **4** 213–25
[2] Zhang M *et al* 2008 Quantitative characterization of viscoelastic properties of human prostate correlated with histology *Ultrasound Med. Biol.* **34** 1033–42
[3] Samani A, Zubovits J and Plewes D 2007 Elastic moduli of normal and pathological human breast tissues: an inversion-technique-based investigation of 169 samples *Phys. Med. Biol.* **52** 1565–76
[4] Sandrin L *et al* 2003 Transient elastography: a new noninvasive method for assessment of hepatic fibrosis *Ultrasound Med. Biol.* **29** 1705–13
[5] Huwart L *et al* 2007 Liver fibrosis: noninvasive assessment with MR elastography versus aspartate aminotransferase-to-platelet ratio index *Radiology* **245** 458–66
[6] Butcher D T, Alliston T and Weaver V M 2009 A tense situation: forcing tumour progression *Nat. Rev. Cancer* **9** 108–22
[7] van Kempen T H, Donders W P, van de Vosse F N and Peters G W 2016 A constitutive model for developing blood clots with various compositions and their nonlinear viscoelastic behavior *Biomech. Model Mechanobiol.* **15** 279–91
[8] Murata H, Shigeto N and Hamada T 1990 Viscoelastic properties of tissue conditioners—stress relaxation test using Maxwell model analogy *J. Oral Rehabil.* **17** 365–75
[9] Jagota A, Argento C and Mazur S 1998 Growth of adhesive contacts for Maxwell viscoelastic spheres *J. Appl. Phys.* **83** 250–9
[10] Schmitt C, Henni A H and Cloutier G 2011 Characterization of blood clot viscoelasticity by dynamic ultrasound elastography and modeling of the rheological behavior *J. Biomech.* **44** 622–9
[11] Magin R L 2006 *Fractional Calculus in Bioengineering* (Danbury, CT: Begell House)
[12] Zhuravkov M A and Romanova N S 2014 Review of methods and approaches for mechanical problem solutions based on fractional calculus *Math. Mech. Solids* **21** 595–621
[13] Carmichael B, Babahosseini H, Mahmoodi S and Agah M 2015 The fractional viscoelastic response of human breast tissue cells *Phys. Biol.* **12** 046001
[14] Mainardi F 2012 Fractional calculus: some basic problems in continuum and statistical mechanics (arXiv:1201.0863)
[15] Podlubny I 1999 *Fractional Differential Equations: an Introduction to Fractional Derivatives, Fractional Differential Equations, to Methods of their Solution and Some of their Applications* vol 198 (San Diego, CA: Academic)
[16] Mattice J M, Lau A G, Oyen M L and Kent R W 2006 Spherical indentation load-relaxation of soft biological tissues *J. Mater. Res.* **21** 2003–10
[17] Nitta N, Shiina T and Ueno E 2003 Hysteresis parameter imaging of soft tissue under quasi-static deformation *2003 IEEE Ultrasonic Symp.* pp 1606–9
[18] Torvik P J and Bagley R L 1984 On the appearance of the fractional derivative in the behavior of real materials *J. Appl. Mech.* **51** 294–8
[19] Sack I, Jöhrens K, Würfel J and Braun J 2013 Structure-sensitive elastography: on the viscoelastic power law behavior of *in vivo* human tissue in health and disease *Soft Matter* **9** 5672–80
[20] Tzikang C 2000 Determining a prony series for a viscoelastic material from time varying strain data NASA Technical Publication NASA/TM-2000 -210123, ARL-TR-2206

[21] Zhang H, Wang Y and Insana M F 2016 Ramp-hold relaxation solutions for the KVFD model applied to soft viscoelastic media *Meas. Sci. Technol.* **27** 025702
[22] Kalyanam S, Yapp R D and Insana M F 2009 Poro-viscoelastic behavior of gelatin hydrogels under compression-implications for bioelasticity imaging *J. Biomech. Eng.* **131** 081005
[23] Lee S and Knauss W G 2002 A note on the determination of relaxation and creep data from ramp tests *Mech. Time-Dep. Mater.* **4** 1–7
[24] Altahhan K N, Wang Y, Sobh N and Insana M F 2016 Indentation measurements to validate dynamic elasticity imaging methods *Ultrason. Imaging* **38** 332–45
[25] Orescanin M, Toohey K S and Insana M F 2009 Quantitative shear wave imaging of cell culture gels *2009 IEEE Ultrasonic Symp.* pp 483–6
[26] Orescanin M and Insana M F 2010 Shear modulus estimation with vibrating needle stimulation *IEEE Trans. Ultrason. Ferroelectr. Freq. Control* **57** 1358–67
[27] Yapp R and Insana M 2009 pH-induced contrast in viscoelasticity imaging of biopolymers *Phys. Med. Biol.* **54** 1089–109
[28] Sridhar M, Liu J and Insana M F 2007 Elasticity imaging of polymeric media *ASME J. Biomech. Eng.* **129** 259–72
[29] Veis A 1964 *The Macromolecular Chemistry of Gelatin* (New York: Academic)
[30] Varghese T, Techavipoo U, Liu W, Zagzebski J A, Chen Q, Frank G and Lee F T Jr 2003 Elastographic measurement of the area and volume of thermal lesions resulting from radiofrequency ablation: pathologic correlation *AJR Am. J. Roentgenol.* **181** 701–7
[31] Orescanin M, Qayyum Q A, Toohey K S and Insana M F 2010 Dispersion and shear modulus measurements of porcine liver *Ultrason. Imaging* **32** 255–66
[32] Sapin-de Brosses E, Gennisson J-L, Pernot M, Fink M and Tanter M 2010 Temperature dependence of the shear modulus of soft tissues assessed by ultrasound *Phys. Med. Biol.* **55** 1701–18
[33] Benech N and Negreira C A 2010 Monitoring heat-induces changes in soft tissues with 1D transient elastography *Phys. Med. Biol.* **55** 1753–65
[34] Gross J 1964 Organization and disorganization of collagen *Biophys. J.* **4** 63–77
[35] Kang T W and Rhim H 2015 Recent advances in tumor ablation for hepatocellular carcinoma *Liver Cancer* **4** 176–87
[36] Chu K F and Dupuy D E 2014 Thermal ablation of tumours: biological mechanisms and advances in therapy *Nat. Rev. Cancer* **14** 199–208
[37] Yarpuzlu B, Ayyildiz M, Tok O E, Aktas R G and Basdogan C 2014 Correlation between the mechanical and histological properties of liver tissue *J. Mech. Behav. Biomed. Mater.* **29** 403–16
[38] Coussot C, Kalyanam S, Yapp R D and Insana M F 2009 Fractional derivative models for ultrasonic characterization of polymer and breast tissue viscoelasticity *IEEE Trans. Ultrason. Ferroelectr. Freq. Control* **56** 715–26
[39] Zhu H-H, Liu L-C, Pei H-F and Shi B 2012 Settlement analysis of the viscoelastic foundation under vertical line load using fractional Kelvin–Voigt model *Geomech. Eng.* **4** 67–78
[40] Zhua H-H, Zhanga C C, Meic G X, Shi B and Gao L 2016 Prediction of one-dimensional compression behavior of Nansha clay using fractional derivatives *Mar. Georesour. Geotechnol.* (doi: 10.1080/1064119X.2016.1217958)
[41] Palmer B M, Tanner B C, Toth M J and Miller M S 2013 An inverse power-law distribution of molecular bond lifetimes predicts fractional derivative viscoelasticity in biological tissue *Biophys. J.* **104** 2540–52
[42] Tong K J and Ebenstein D 2015 Comparison of spherical and flat tips for indentation of hydrogels *J. Met.* **67** 713–9
[43] Oyen M L 2015 Nanoindentation of hydrated materials and tissues *Curr. Opin. Solid State Mater. Sci.* **19** 317–23
[44] Isaza J and Ramirez J 2015 Incidence of temperature and indenter diameter on the mechanical response of skin during indentation test *Proc. Eng.* **110** 45–50